Sensors and Actuators B 216 (2015) 349–357

Contents lists available at ScienceDirect

Sensors and Actuators B: Chemical

journal homepage: www.elsevier.com/locate/snb

Improved self-assembled thiol stationary phases in microfluidic gas separation columns

Hamza Shakeel[a], Dong Wang[b], James R. Heflin[b], Masoud Agah[a,*]

[a] VT MEMS Lab Bradley Department of Electrical & Computer Engineering, Virginia Tech, Blacksburg, VA 24061, USA
[b] Department of Physics, Virginia Tech, Blacksburg, VA 24061, USA

ARTICLE INFO

Article history:
Received 12 January 2015
Received in revised form 10 March 2015
Accepted 19 March 2015
Available online 16 April 2015

Keywords:
Micro gas chromatography
Semipacked columns
Gas–solid stationary phase
Gold nanoparticles
Evaporated gold
Layer-by-layer self-assembly

ABSTRACT

Semipacked columns (SPCs) with integrated micropillars have been characterized for high chromatographic efficiencies and fast separations. In this article, high-yield and stable alkane thiol based stationary phase coating methods are presented for SPCs. Briefly, a new three step (anisotropic, O_2 plasma, and isotropic) etching method is first developed in order to improve metal lift-off by producing a 3-dimensional undercutting profile inside deep etched SPCs. This innovative fabrication scheme is used for 1 m-long, 220 μm-deep, 190 μm-wide SPCs with circular micropillars of 20 μm-diameters and 42 μm-post spacing. Two different thin gold film deposition techniques are utilized for microcolumns (1) a wafer-level physical vapor deposition, and (2) a device level layer-by-layer (LbL) self-assembly of gold nanoparticles (3.2 nm diameter). After gold film deposition and metal lift-off, the surface of the patterned gold layer is functionalized with a 2 mM octadecanethiol ($C_{18}H_{37}SH$) solution for chromatographic separations. Both kinetic (Golay plots) and thermodynamic (Van't Hoff plot) properties of thiol-functionalized gold phases are studied. The significance of SPCs, for faster analysis, is also validated by achieving baseline separation of a straight chain alkane mixture, containing high boilers (174 °C to 287 °C), within 45 s.

1. Introduction

The miniaturization of different gas chromatography (GC) components, such as pre-concentrators/injectors [1–7], separation columns [8–13], and detectors [14–19], enables the realization of a field portable system [20–28] for real-time sample analysis. Chip-based GC separation columns, realized through planar microfabrication of silicon–glass substrates, have been the main subject of several recent research studies. Apart from separation capabilities, certain critical GC functionalities such as temperature programming [29,30] and flow rate sensing [13] have also been integrated on the same silicon–glass chip. The high thermal conductivity of silicon (149 W/m K) [31], shorter column lengths (0.25 m to 3 m) [32–34], and smaller chip sizes (typically 2 cm × 2 cm) [12,35] along with new stationary phase coating materials result in low-power consumption (<100 mW) [12] and rapid temperature programming rates (60 °C/s) [32] enabling faster (less than a minute) as well as efficient (>10,000 plates/m) separations [35,36]. Moreover, the use of standard cleanroom fabrication processes, mainly lithography and plasma based dry etching, has also enabled the realization of producing separation channels with arbitrary shapes and geometrical patterns. This is not possible with the conventional manufacturing techniques employed for glass capillary columns. These innovative designs include partially buried micro-columns [37], low-mass oxy-nitride semi-circular suspended columns [38], width-modulated rectangular columns [39], and SPCs with embedded micron-sized pillars [30,35,40–45]. Among these designs SPCs, invented at Virginia Tech MEMS lab [40], have attracted considerable attention due to their improved separation efficiency, sample capacity, and speed of analysis compared to regular open channel columns.

Both static and dynamic gas–liquid phase coating methods [34,35,46], specifically tailored for microchip coating, have been successfully employed for silicon–glass microchannels. The work on micro-electro-mechanical-systems (MEMS) compatible gas–solid stationary phase coating methods has been the focus of continuous research during the last decade. Different research studies have demonstrated the separation capabilities of carbon nanotubes (CNTs) [32], sputtered oxides [29,42,43], atomic layer deposited alumina [41,47], silica nanoparticles (SNPs) [48,49], and monolayer-protected-gold (MPG) [33,36] based solid adsorbent films for silicon microcolumns. Briefly, Stadermann et al. [32], using chemical vapor deposition, integrated single-walled CNTs into a 100 μm × 100 μm channel to achieve ultrafast separation of four

* Corresponding author.
E-mail address: agah@vt.edu (M. Agah).

http://dx.doi.org/10.1016/j.snb.2015.03.107
0925-4005/

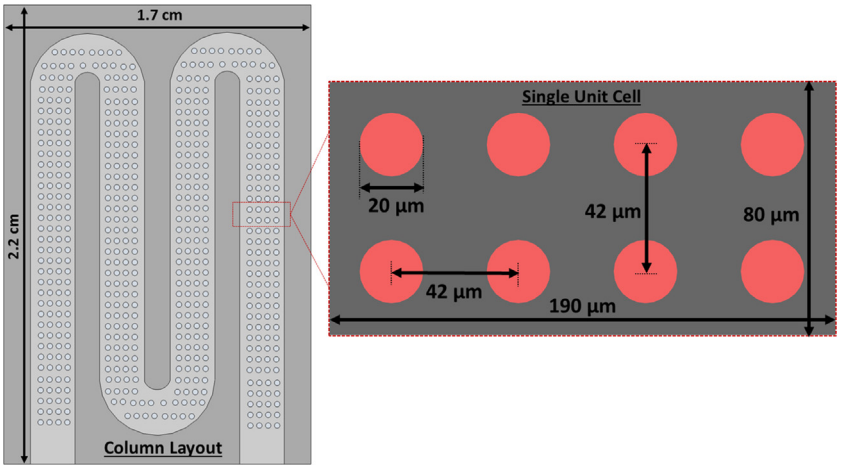

Fig. 1. Layout (top view) of a 1 m-long semipacked column showing critical dimensions.

compounds in 1 s using fast temperature ramp rates. Haudebourg et al. [29] employed a wafer-level sputtering mechanism to coat thin films of different adsorbent materials (silica and graphite) into SPCs (100 μm-deep channel and 10 μm × 10 μm square micropillars) for oilfield applications. Similarly, our research group has previously shown the separation capabilities of SNPs (coated using layer-by-layer self-assembly) [48] and wafer-level atomic layer deposited/silane functionalized alumina thin films [43] for different channel geometries. Furthermore, we have shown different microfabrication methodologies for depositing thin layers of gold inside high-aspect-ratio (HAR) microcolumns followed by a thiol functionalization step. In this article, we introduce a new high-yield metal patterning process for HAR structures, using a single layer positive photoresist (PR) and a three stage (anisotropic, plasma clean and isotropic) etching process to generate an undercut profile. Therefore, when metal is deposited, the film is discontinuous over the deep etched (>200 μm) micron-sized features enabling easy removal of PR and leaving behind a well-defined metal thin film. Two different gold deposition techniques are successfully demonstrated for 220 μm-deep SPCs, (1) a wafer-level electron-beam evaporation (physical vapor deposition), and (2) a LbL self-assembly of gold nanoparticles (GNPs). Compared to our previous effort for coating functionalized GNPs [50], this new LbL coating scheme was found to be highly stable under GC testing conditions mainly due to shorter coating steps (~3 min) and calcination at higher temperature. Moreover, comparatively our earlier work on self-patterned gold-electroplated columns with MPG phases required very high processing temperature (950 °C) and also afforded high fabrication complexity [33,51]. The separation capabilities of the proposed gold coated/thiol functionalized SPCs are demonstrated with high-speed separation of an alkane mixture. Fig. 1 shows the detailed column and microchannel layout profile of 1 m-long SPCs utilized for validating our newly proposed fabrication method.

2. Experimental

2.1. Materials and reagents

Microcolumn fabrication took place on 4″ silicon (500 μm thick, p-type, ⟨1 0 0⟩, 0–100 Ω cm) and Borofloat® glass (700 μm thick ± 7 μm) wafers purchased from University Wafers and Corsix Precision Glass, respectively. Deactivated fuse silica glass capillary tubing (outer diameter 200 μm and internal diameter 100 μm), was obtained from Polymicro Technologies. A two part epoxy adhesive (MS-907) was purchased from Miller Stephson. All the chemicals used for GC testing (analytical standard with ≥99.8% purity), LbL coating (polycation polyallylamine hydrochloride (PAH)), self-assembly (octadecanethiol) and glass surface deactivation (octadecyltrichlorosilane (ODTS)) were obtained directly from Sigma-Aldrich. Ultrahigh pure helium (>99.99%) was used as the carrier gas for all GC experiments and purchased from Air Gas Ltd, USA. Methane gas (99% grade) used for calculating column dead time, linear velocity, and capacity factors (k') was acquired from Matheson Trigas, Ohio. Gold nanoparticle suspension (MesoGold™, 3.2 nm average diameter and 20 ppm concentration in pure water) was purchased from Purest Colloid Inc.

2.2. Instrumentation and testing

A bench-top Agilent GC system (7890) equipped with an autosampler (7359A), an electronic pressure controller, and a flame ionization detector (FID) was used for performing all the chromatographic tests. Both inlet and detector temperatures were maintained at 280 °C for all the tests.

2.3. Fabrication

The fabrication of a modified lift-off process for metal deposition and surface functionalization requires multiple stages and is illustrated step-by-step in Fig. 2. This process can be broadly categorized into column fabrication, thin gold film deposition (either e-beam or LbL), anodic bonding, and column functionalization.

2.3.1. Column fabrication

The fabrication of microcolumns starts with a silicon wafer priming step using hexamethyldisilazane (HMDS); an adhesion promoter for the photoresist (PR), followed by substrate heating at 110 °C for 5 min. After which the HMDS-primed wafer is spin coated with a positive AZ® 9260 PR (i-line broadband PR by AZ Electronic Materials) at 500 rpm for 15 s and 2000 rpm for 1 mi. Following this, the PR-coated wafer is soft-baked at 110 °C for 90 s. This process is conducted to reduce the solvent content in the PR and further improve wafer adhesion with PR. Next the soft-baked wafer is exposed for 55 s using an ultra-violet light source with a mask aligner (Karl Suss, MA-6) system followed by development in an aqueous AZ400 K (3:1) developer solution. In the proceeding step, the thickness of PR (~8.8 μm) is characterized with a surface profilometer (DekTak) and further verified through SEM imaging (Fig. 3a). It is important to note that the wafer is not hard-baked after PR development; this is found to further improve the metal

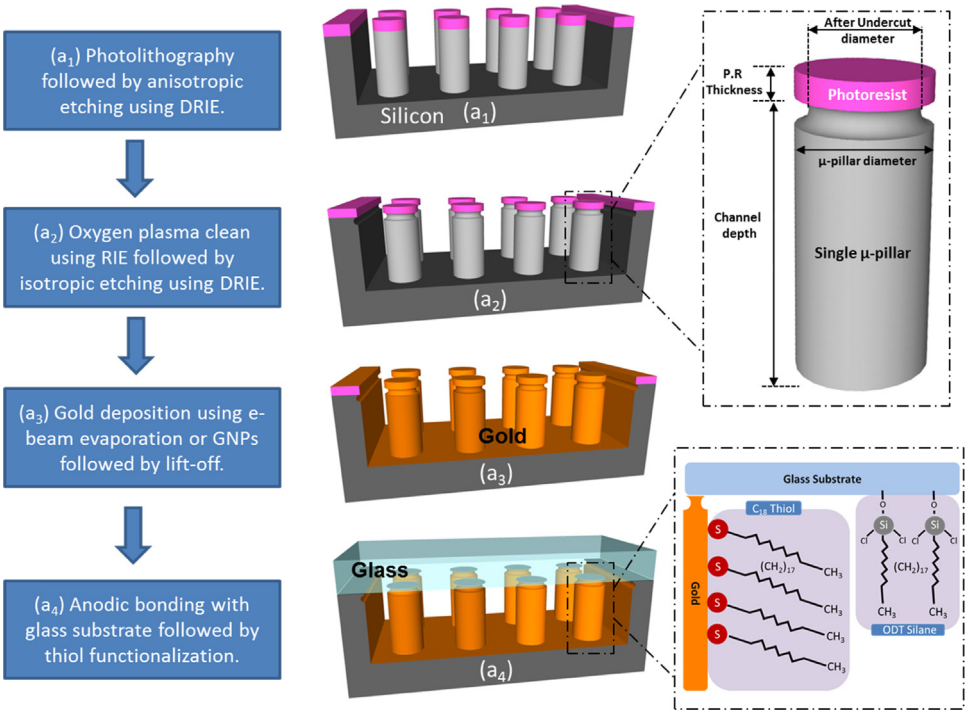

Fig. 2. Process flow for the fabrication of semipacked columns with a three-step etching technique to produce undercut profile.

lift-off process. The three-step dry etching of SPCs is explained in detail below.

2.3.1.1. Anisotropic etching. First, the PR-patterned wafer is anisotropically etched for 48 min at 0 °C in a deep reactive ion etching (DRIE) system (Alcatel AMS-100). This is conducted using a sequential flow of etch (SF_6) and passivation (C_4F_8) gases; known as a standard Bosch™ process [52] (etching conditions mentioned in supplementary material Table 1). Although the micropillars (μ-pillars) are designed with 20 μm-diameters (Fig. 1), anisotropic etching results in a ~3 μm lateral etching eventually producing ~17 μm μ-pillars (Fig. 3b).

2.3.1.2. Oxygen plasma etch. In the second step, the anisotropically etched silicon wafer is etched for 2 min (O_2 plasma, supplementary material Table 2) using a Trion reactive ion etching (RIE) system to remove the passivation layer deposited on the etched surfaces during Bosch™ process. It is important to note that without this step, undercutting of silicon is not possible since all the vertical surfaces are covered with passivated polymer from the first step. Similarly, a low-powered RIE system is found to be more suitable compared to

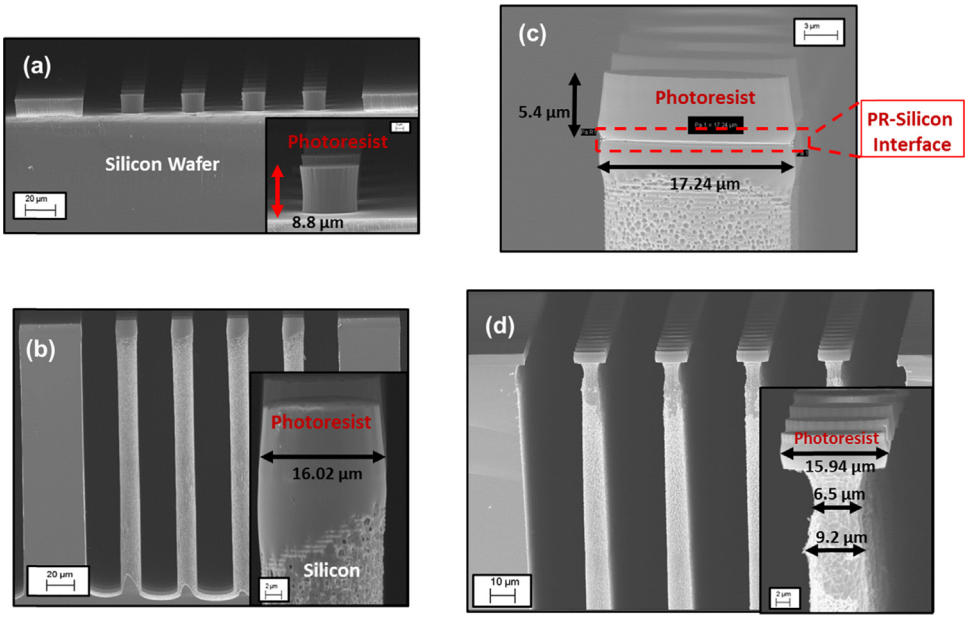

Fig. 3. SEM micrographs of a device during different fabrication steps: (a) after lithography, (b) after anisotropic etching using DRIE, (c) O_2 plasma etch of passivation polymer in Trion RIE, and (d) under-etching of high-aspect ratio micropillars in DRIE using isotropic etching. Insets show the images at magnified scale.

DRIE system for this step. Moreover, it has also been found during SEM imaging that the interface between PR and the top silicon surface is also cleared from residual PR/passivation polymer as shown in Fig. 3c. This helps in achieving the required undercut. It is important to mention here that a single wafer was also fabricated by terminating the process at this point but no improvement in metal lift-off was observed.

2.3.1.3. Isotropic etching. In the last step, the undercutting of HAR microstructures is carried out using an isotropic etch [52] recipe with a fluorine based chemistry (SF_6) at 0 °C inside a DRIE chamber for 2 minutes (Table 3, supplementary material, shows etch conditions utilized for achieving the desired undercut). The overall thickness of the μ-pillar is further reduced by ~3 μm due to isotropic etching. The detailed etch profile after 3-dimensional undercutting is shown in the Fig. 3d. Keeping the PR intact, thin gold film deposition is carried out in the next steps.

2.4. Gold film deposition

The self-patterning of thin gold layers inside the etched SPCs is achieved by two methods, (1) a wafer-level physical vapor deposition (PVD) using an e-beam evaporation source, and (2) a device level LbL method using GNPs suspension (Fig. 4). The details of each gold deposition method are provided below

2.4.1. e-Beam evaporation

The PVD deposition of the thin film starts with placing an etched silicon wafer on a rotating platen inside the PVD-250 (Kurt Lesker) chamber as shown in Fig. 4a. In short, the chamber is pumped down to a base pressure of 3×10^{-6} torr. Then, an e-beam power source is turned-on and is directed towards the target (anode) with the help of magnetic deflectors. The high energy e-beam bombards the surface of the target material causing it to transform into a gaseous phase. This gaseous anode material nucleates on the surface of the wafer forming a thin film with the desired thickness. Since the adhesion of the gold layer to silicon is poor, a thin layer (~25 nm) of chrome is first deposited on the surface followed by 240 nm thin gold film deposition (1 Å/s rate). After gold deposition, the metal lift-off process is accomplished by immersing the wafer into acetone followed by a short agitation (5 min) in a sonication bath. The average film thickness of the gold layer was found to be 239 nm (Fig. 5).

2.4.2. LbL self-assembly of GNPs

For LbL deposition, the etched silicon wafer, with PR intact, is first diced into the individual devices. The GNP thin film is deposited via the LbL ionic self-assembly method recently demonstrated/optimized for μGC by our group with SNPs [48]. Each device is first attached to a glass microscope slide with a double-sided scotch tape and placed in an automatic dipping system (StratoSequence VI Robot, nanoStrata, Inc.). In the current scheme, the LbL coating starts by alternately immersing each device into an aqueous 10 mM PAH (pH = 4.0 ± 0.1, stirred overnight) and GNPs colloid (used as received) solution for 3 min. Each coating cycle results in a single bilayer (BL) and is formed by an attractive electrostatic bonding of a positively-charged PAH layer and a negatively-charged GNP (−40 mV zeta potential) layer. A single 3 min coating cycle of PAH or GNPs is followed by three 45 s rinsing steps in between using deionized (DI) water to remove any excess material coated during the prior step (Fig. 4b). The process is terminated after the desired number of BLs are deposited inside the microchannel. In the current work, SPCs are coated with 30, 50 and 100 bilayers. After LbL coating, each device is first dried with a low flux nitrogen gas and dipped in acetone followed by sonication for 5 min to achieve the metal lift-off. Similar to our earlier studies, the devices were placed in an oven at 500 °C for 4 h to burn the PAH, leaving behind only the evenly distributed GNPs coating with nanoscale roughness on the desired microsurfaces.

The robustness of the newly developed scheme is validated by fabricating 12 gold-coated columns across different wafers producing a fabrication yield of ~91%.

2.5. Anodic bonding and functionalization

Following thin gold film deposition, each micro column is sealed with a Borofloat® glass substrate (400 °C, 1250 V, 45 min) using a custom made anodic bonding station. Approximately 30 cm-long glass capillary tubing is glued using Epoxy-907 to each port of the silicon-glass chip, providing a fluidic interface between the chip and GC oven.

Surface deactivation using silylating agents improves the inertness of the glass substrate and limits the residual activity of surface silanol (hydroxyl) groups to reduce the peak deformation/tailing during chromatographic separation. Similar to our previous findings to improve the peak symmetry, each microcolumn is first treated with a 10 mM octadecyltrichlorosilane (diluted in toluene) for 12 h at room temperature [53]. Following glass deactivation, the self-assembly of octadecanethiol thiol on a gold surface is exploited to create a gas–solid stationary phase [54].

$$C_{18}H_{37}SH + Au^0 \xrightarrow{SAM} [C_{18}H_{37}S^- + Au^+] + 1/2H_2$$

For thiol self-assembly, each column is filled with a 2 mM octadecanethiol ($C_{18}H_{37}SH$) in hexane, sealed at both ends using septa (made of high grade silicone) and kept at room temperature for 6 h. Fig. 2 shows the chemical structure of both self-assembled C_{18} thiol on gold and ODTS on glass surfaces.

3. Results and discussion

The contribution of the gold films deposited using methods described in the last section is first tested before any functionalization steps. Fig. 6 clearly demonstrates that GNP layer alone (evaporated gold film shows similar behavior but not shown) is inadequate for GC separations. Before performing any chromatographic separations on functionalized columns, each device is first purged with a constant flow of dry nitrogen for 30 min. Each chip is then connected to a conventional GC oven and slowly heated from room temperature to 150 °C (2 °C/min) with a constant inlet pressure of 7.5 psi until a stable signal baseline is observed. Fig. 6 also shows that SPCs with thiol functionalized GNPs (100 BLs) are able to separate a simple alkane mixture. It is important to note that 30 and 50 BL GNP columns performed poorly in comparison to those having 100 BLs due to incomplete coverage of the etched channels with nanoparticles. Therefore, only columns coated with 100 BL GNP were used for further GC analysis in addition to evaporated gold columns. The thickness of 100 BLs was measured to be ~300 nm using SEM (not shown).

3.1. Column performance

In this work, both kinetic and thermodynamic properties of microfabricated columns with thiol phases are evaluated using Golay and Van't Hoff plots. The kinetic performance of the separation columns is typically evaluated using a metric known as a height-equivalent-to-a-theoretical-plate (HETP). The Van Deemeter equation (1) theoretically relates different sources of column peak band broadening to HETP (cm) [55].

$$\mathrm{HETP} = A + \frac{B}{u} + (C_S + C_M) \times \bar{u} \quad (1)$$

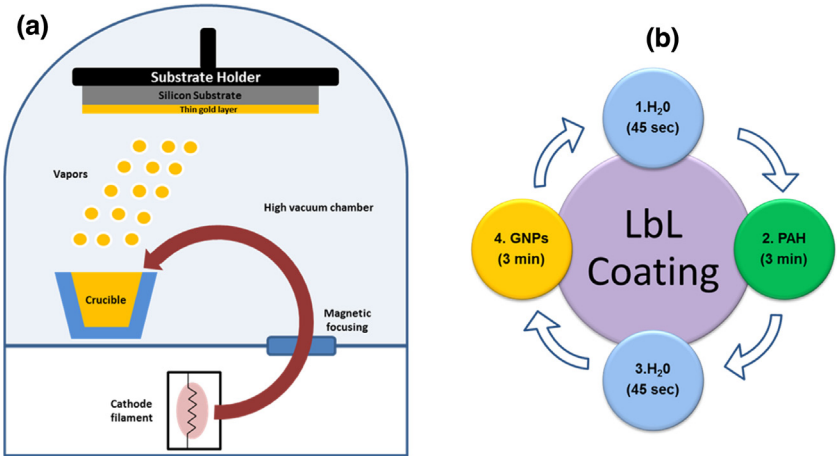

Fig. 4. Schematics of (a) an e-beam evaporation system during wafer coating and (b) a LbL coating scheme for thin-gold film deposition using GNPs and PAH.

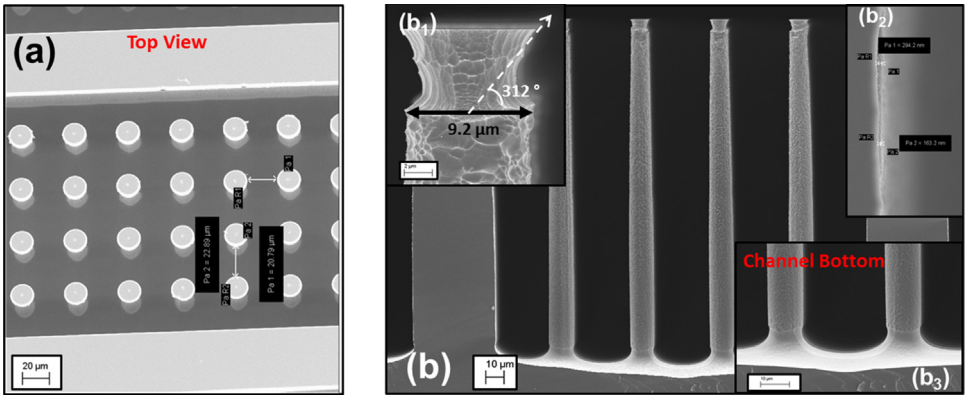

Fig. 5. SEM micrographs of a microchannel after photoresist removal in acetone (a) top view and (b) channel cross-section. Inset (b_1) shows pillar-top at magnified scale, (b_2) shows gold thickness on sidewall and (b_3) shows slight undercut at the bottom of microchannel.

here $\bar{u}$ (cm/s) is the average linear carrier gas velocity. The A (cm) term, arising due to eddy diffusion or multiple paths, is only significant in packed columns and has minimal effect for SPCs properly designed with uniform gas flow paths [40]. The B ($cm^2\ s^{-1}$) term reflects the molecular diffusion of solute molecules in the carrier gas. The C_S and C_M (s) terms represent the resistance due to mass transfer in stationary and mobile phases, respectively. The HETP is typically calculated experimentally from a chromatogram using relationships (2) and (3) [55]

$$\mathrm{HETP}_{\mathrm{eff}} = \frac{L}{N_{\mathrm{eff}}} \tag{2}$$

where L is the length of the column and N_{eff} is the effective plate number, taking into account dead volume in the column and evaluated using [55]

$$N_{\mathrm{eff}} = \left(\frac{t_r - t_M}{w_{1/2}}\right)^2 \tag{3}$$

where t_M is known as the dead or hold-up time calculated from an unretained methane peak, t_r is the retention time and $w_{1/2}$ is the peak width at half the height of a selected solute probe, typically a straight chain alkane. It is necessary to account for the dead time in calculating efficiency (plate number) for microcolumns,

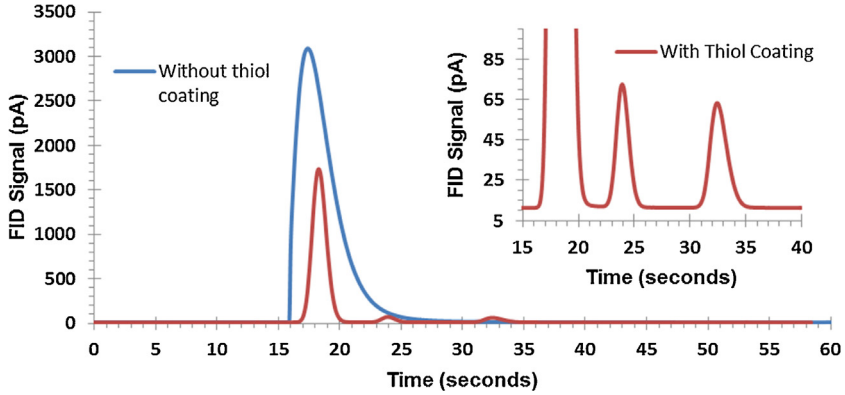

Fig. 6. Separation performance of an uncoated and a thiol-coated GNPs column using *n*-nonane and *n*-decane (diluted in dichloromethane) as probes. Column tested at 50 °C, 5 psi head pressure, 200:1 split ratio, and 0.1 µL sample injection.

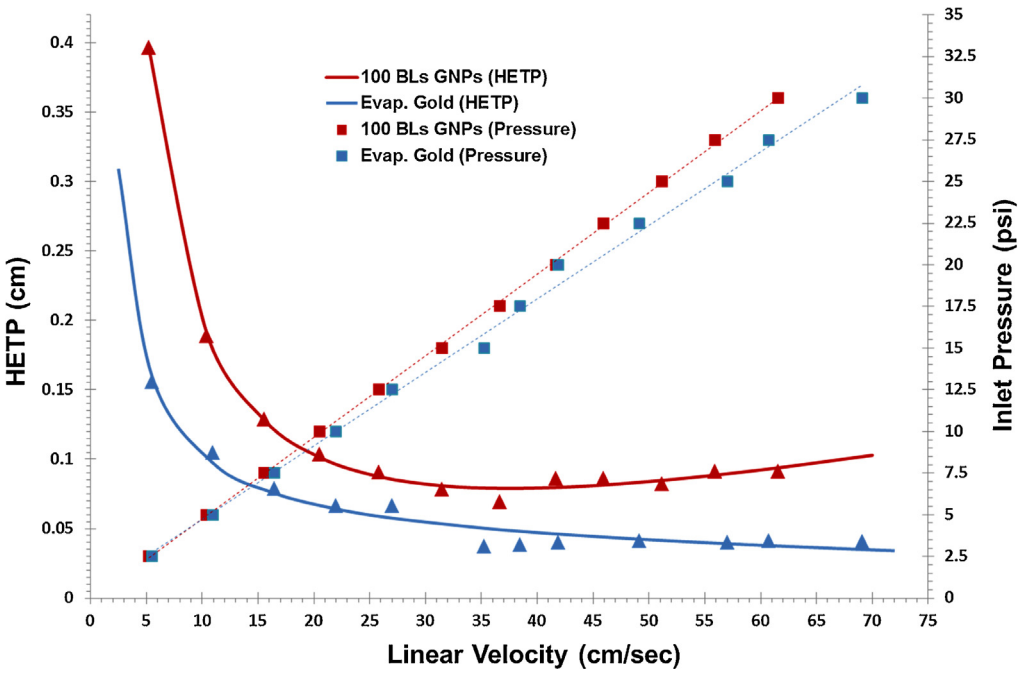

Fig. 7. Golay plots of evaporated gold (blue) and GNPs (red) based SPCs using *n*-decane (3300 ppm) as a marker at isothermal condition (50 °C) with 0.1 μL sample injection and 200:1 split ratio (head pressure varied from 2.5 psi to 30 psi). Triangular markers represent HETP (solid lines) values, while square markers represent pressure (dotted lines).

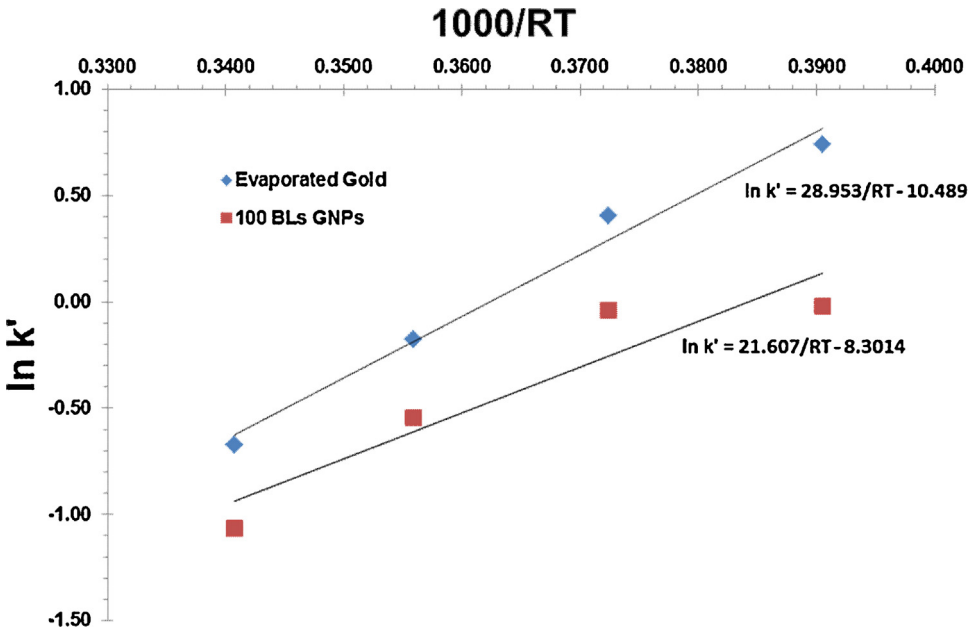

Fig. 8. Thermodynamic properties of thiol functionalized evaporated gold and GNPs coated SPCs using Van't Hoff plots. *n*-Decane is used as a probe with each column tested from 35 °C to 80 °C at 7.5 psi head pressure. Methane vapor is used to calculate the dead times/capacity factors (k') corresponding to different temperatures with $R = 8.314$ J/K mol.

especially with very narrow widths and comparable lengths of interfacing capillary tubing resulting in a large dead volume. Fig. 7 shows Golay plots of both GNPs and evaporated gold SPCs, generated using *n*-decane as a probe under isothermal conditions (35 °C, 0.1 μL injection volume, split ratio 200:1). The optimum linear carrier gas velocity of 37 cm/s is calculated providing a minimum $HETP_{eff}$ value of 0.0376 cm (evaporated gold). It is desirable to operate columns above linear velocities in order to reduce the analysis time. The flatness of the HETP curve above optimum linear velocities, a characteristic of SPCs, shows that there is small loss in separation efficiencies when operating the columns at high velocities. Moreover, the flatness of the curve at higher velocities demonstrates that the effect of mass transfer terms (C_S and C_M) is smaller than the B term, which is desirable for high speed operations. Fig. 7 also shows a linear correlation between the inlet/head pressure and the corresponding calculated linear carrier gas velocity. Both gold-thiol coatings were found to be highly stable for six months under GC testing conditions (maximum pressure of 30 psi and temperature up to 175 °C) and after multiple sample injections (2 0 0).

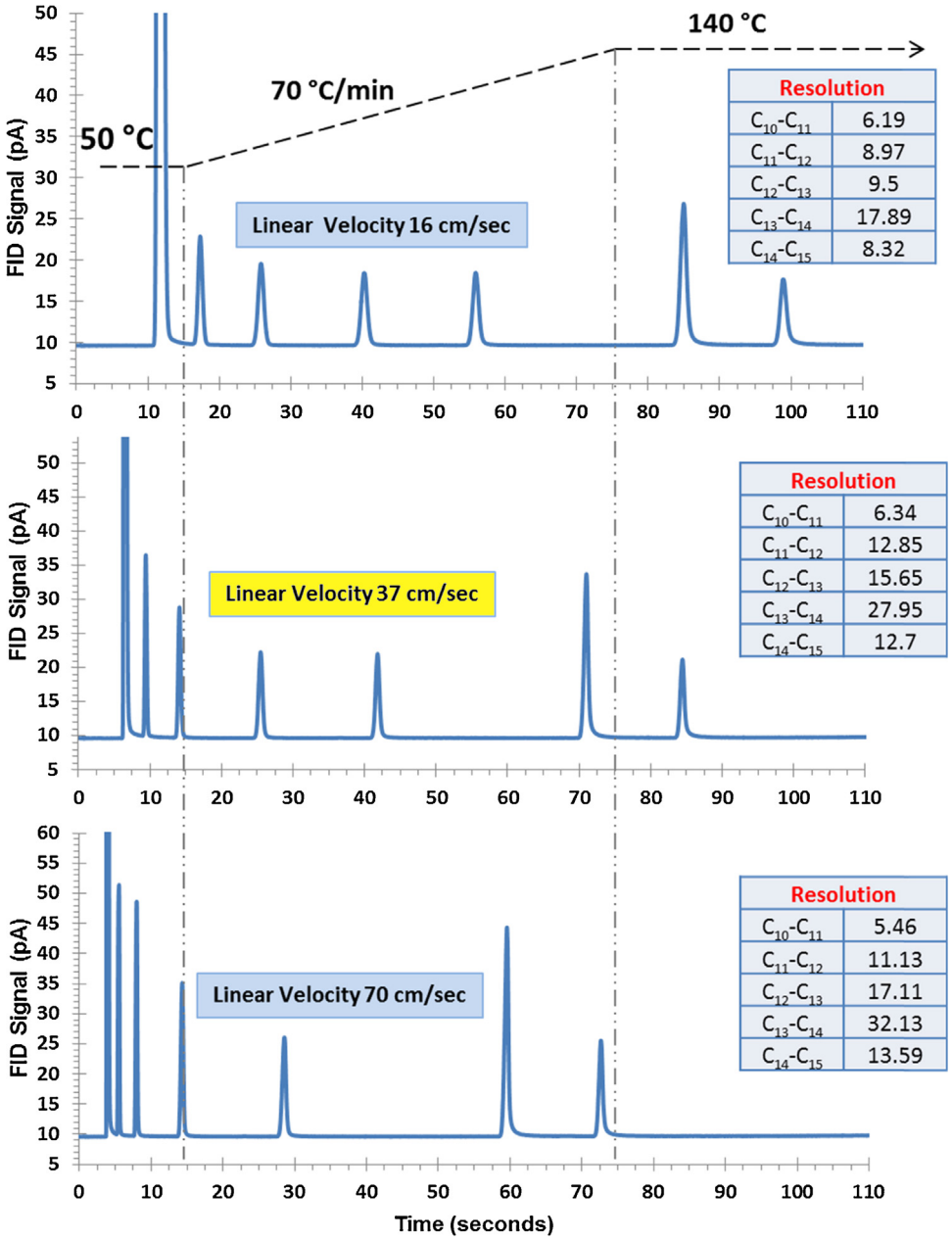

Fig. 9. Separation performance of an evaporated gold coated/thiol functionalized column at three different linear velocities, 37 cm/s (optimum), 17 cm/s (below optimum) and 70 cm/s (above optimum). Compound indentification (in order of elution), dicholoromethane, *n*-decane, *n*-undecane, *n*-dodecane, *n*-tridecane, *n*-tetradecane and *n*-pentadecane. Temperature programming curves are superimposed on each chromatogram. GC testing performed under a constant flow mode.

Thermodynamic properties of thiol functionalized gold films were evaluated using Van't Hoff plots (Fig. 8). The plots, generally linear ($R^2 > 0.87$ and $R^2 > 0.96$), are generated between 35 °C to 80 °C using *n*-decane (diluted in dichloromethane) as a probe and dead-time is yet again calculated from an unretained methane vapor. From the Van't Hoff plots, the values of the standard adsorption heat for evaporated gold ($|\Delta_r H^{\theta}|$=28.95 kJ/mol) column is close to that of a 100 BLs GNPs ($|\Delta_r H^{\theta}|$=21.60 kJ/mol) coated SPCs meaning evaporated gold coated columns retain slightly better than GNPs and thermodynamically very similar. These values are lower than that calculated for CNTs ($|\Delta_r H^{\theta}|$=46.2 kJ/mol) [32] based coating also using *n*-decane as a marker. This means that the retention of gold-thiol based stationary phases is lower than that of CNTs based phases. The higher retention of CNTs could be attributed to the higher surface area of nanotubes due to the height (1.7 μm) of a nanotube mat. The retention of gold-thiol coating could also be improved further by increasing the thiol coating time from 6 h to 12 h or more.

3.2. Chromatographic separations

The separation capability of both functionalized gold phases is evaluated using a simple straight chain alkane mixture with 7200 ppm concentration of each compound. Since the separation behavior of both phases are very similar, only results of evaporated gold coated SPCs, showing better retention than GNPs coated devices, are presented here. It has earlier been reported that C_{18}-thiol based phases are able to only selectively resolve straight chain alkane based mixtures [53]. Therefore, only straight-chain alkanes are used for GC separations. In order to show the significance of using SPCs, the mixture is tested at three different carrier gas velocities (16 cm/s, 37 cm/s and 70 cm/s) as shown in Fig. 9. Moreover,

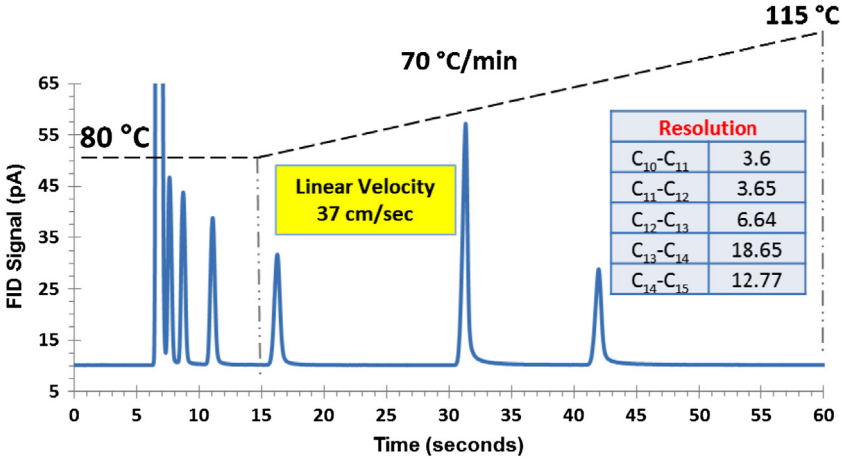

Fig. 10. Separation performance of an evaporated gold coated/thiol functionalized column at optimum linear velocity (37 cm/s) at higher initial temperature 80 °C. GC testing performed under constant flow mode.

the peak-to-peak resolution (R_S) between adjacent analyte peaks is also evaluated using [55]

$$R_S = 2 \times \left(\frac{t_{rb} - t_{ra}}{w_{rb} + w_{ra}} \right) \quad (4)$$

where, t_{ra} and t_{rb} correspond to retention times and w_{ra} and w_{rb} represent the peak widths at base of corresponding compounds a and b. From Fig. 9, it is clear that SPCs operating below optimum carrier gas velocity take 100 s to complete the separation, while at higher linear velocity (70 cm/s) the separation is completed within 75 s. Moreover, all the peaks are baseline separated ($R_S > 1.5$) with loss of resolution between the first few peaks being relatively small. In order to further reduce the analysis time, without significantly effecting peak-to-peak resolution, the initial operating temperature of SPCs is increased from 50 °C to 80 °C. Fig. 10 shows that the separation of the same mixture could be achieved within 45 s with baseline resolution, thus significantly reducing the total analysis time.

4. Conclusion

In conclusion, we present improved gold-thiol coating schemes for SPCs. The proposed fabrication method is validated for both evaporated gold and thin GNPs films (deposited using LbL self-assembly). The chromatographic performance of thiol functionalized evaporated gold and 100 BLs of GNPs thin films is found to be comparable, with evaporated gold coated columns demonstrating slightly better separation efficiencies. Moreover, thermodynamically both phases show similar behavior with evaporated gold film showing slightly better retention. Fast analysis (45 s) for high boilers is achieved utilizing the proposed scheme for evaporated gold SPCs. Evaporated gold thiol based stationary phases provide a wafer level coating scheme. Similarly the availability of different thiol chemistries could further provide selective chemical separations. We also envision that this newly developed method could also be employed for patterning thicker stationary phase films (up to 1 μm) inside deep channels (≤250 μm).

Acknowledgment

All the SEM images were taken at the Institute of Critical Technology and Applied Science, Nanoscale Characterization and Fabrication Laboratory (ICTAS-NCFL), Virginia Tech. This work was supported primarily by the National Science Foundation under award number ECCS-1002279.

Appendix A. Supplementary data

Supplementary data associated with this article can be found, in the online version, at http://dx.doi.org/10.1016/j.snb.2015.03.107

References

[1] T. Sukaew, H. Chang, G. Serrano, E.T. Zellers, Multi-stage preconcentrator/focuser module designed to enable trace level determinations of trichloroethylene in indoor air with a microfabricated gas chromatograph, Analyst 136 (2011) 1664–1674.
[2] M. Akbar, M. Agah, A microfabricated propofol trap for breath-based anesthesia depth monitoring, IEEE J. Microelectromech. Syst. 22 (2013) 443–451.
[3] T. Wei-Cheng, S.W. Pang, L. Chia-Jung, E.T. Zellers, Microfabricated preconcentrator-focuser for a microscale gas chromatograph, IEEE J. Microelectromech. Syst. 12 (2003) 264–272.
[4] I. Gràcia, P. Ivanov, F. Blanco, N. Sabaté, X. Vilanova, X. Correig, L. Fonseca, E. Figueras, J. Santander, C. Cané, Sub-ppm gas sensor detection via spiral μ-preconcentrator, Sens. Actuators, B: Chem. 132 (2008) 149–154.
[5] M. Akbar, D. Wang, R. Goodman, A. Hoover, G. Rice, J.R. Heflin, M. Agah, Improved performance of micro-fabricated preconcentrators using silica nanoparticles as a surface template, J. Chromatogr. A 1322 (2013) 1–7.
[6] G. Serrano, T. Sukaew, E.T. Zellers, Hybrid preconcentrator/focuser module for determinations of explosive marker compounds with a micro-scale gas chromatograph, J. Chromatogr. A 1279 (2013) 76–85.
[7] B. Alfeeli, D. Cho, M. Ashraf-Khorassani, L.T. Taylor, M. Agah, MEMS-based multi-inlet/outlet preconcentrator coated by inkjet printing of polymer adsorbents, Sens. Actuators, B: Chem. 133 (2008) 24–32.
[8] G. Serrano, S.M. Reidy, E.T. Zellers, Assessing the reliability of wall-coated microfabricated gas chromatographic separation columns, Sens. Actuators, B: Chem. 141 (2009) 217–226.
[9] D. Gaddes, J. Westland, F.L. Dorman, S. Tadigadapa, Improved micromachined column design and fluidic interconnects for programmed high-temperature gas chromatography separations, J. Chromatogr. A 1349 (2014) 96–104.
[10] H. Hao-Chieh, K. Hanseup, Miniature circulatory column system for gas chromatography, in: Micro Electro Mechanical Systems (MEMS), 2014 IEEE 27th International Conference on, 2014, pp. 1007–1010.
[11] A. Bhushan, D. Yemane, E.B. Overton, J. Goettert, M.C. Murphy, Fabrication and preliminary results for LiGA fabricated nickel micro gas chromatograph columns, IEEE J. Microelectromech. Syst. 16 (2007) 383–393.
[12] M. Agah, J.A. Potkay, G. Lambertus, R. Sacks, K.D. Wise, High-performance temperature-programmed microfabricated gas chromatography columns, J. Microelectromech. Syst. 14 (2005) 1039–1050.
[13] M. Agah, G.R. Lambertus, R. Sacks, K. Wise, High-speed MEMS-based gas chromatography, J. Microelectromech. Syst. 15 (2006) 1371–1378.
[14] B.C. Kaanta, H. Chen, X. Zhang, A monolithically fabricated gas chromatography separation column with an integrated high sensitivity thermal conductivity detector, J. Micromech. Microeng. 20 (2010) 055016.
[15] S. Narayanan, M. Agah, Fabrication and characterization of a suspended TCD integrated with a gas separation column, J. Microelectromech.Syst. 22 (2013) 1166–1173.
[16] S. Narayanan, G. Rice, M. Agah, A micro-discharge photoionization detector for micro-gas chromatography, Microchim. Acta 181 (2014) 493–499.
[17] F.I. Bohrer, E. Covington, C.a. Kurdak, E.T. Zellers, Characterization of dense arrays of chemiresistor vapor sensors with submicrometer features and patterned nanoparticle interface layers, Anal. Chem. 83 (2011) 3687–3695.

[18] S. Zampolli, I. Elmi, J. Stürmann, S. Nicoletti, L. Dori, G.C. Cardinali, Selectivity enhancement of metal oxide gas sensors using a micromachined gas chromatographic column, Sens. Actuators, B: Chem. 105 (2005) 400–406.
[19] K. Reddy, L. Jing, M.K.K. Oo, F. Xudong, Integrated separation columns and Fabry–Perot sensors for microgas chromatography systems, J. Microelectromech. Syst. 22 (2013) 1174–1179.
[20] Q. Yutao, Y.B. Gianchandani, A micro gas chromatograph with integrated bi-directional pump for quantitative analyses, in: Micro Electro Mechanical Systems (MEMS), 2014 IEEE 27th International Conference on, 2014, pp. 294–297.
[21] S. Zampolli, I. Elmi, F. Mancarella, P. Betti, E. Dalcanale, G.C. Cardinali, M. Severi, Real-time monitoring of sub-ppb concentrations of aromatic volatiles with a MEMS-enabled miniaturized gas-chromatograph, Sens. Actuators, B: Chem. 141 (2009) 322–328.
[22] S.K. Kim, H. Chang, E.T. Zellers, Microfabricated gas chromatograph for the selective determination of trichloroethylene vapor at sub-parts-per-billion concentrations in complex mixtures, Anal. Chem. 83 (2011) 7198–7206.
[23] Y. Qin, Y.B. Gianchandani, iGC2: an architecture for micro gas chromatographs utilizing integrated bi-directional pumps and multi-stage preconcentrators, J. Micromech. Microeng. 24 (2014) 065011.
[24] R.-S. Jian, L.-Y. Sung, C.-J. Lu, Measuring real-time concentration trends of individual VOC in an elementary school using a sub-ppb detection μGC and a single GC–MS analysis, Chemosphere 99 (2014) 261–266.
[25] J. Liu, J.H. Seo, Y. Li, D. Chen, K. Kurabayashi, X. Fan, Smart multi-channel two-dimensional micro-gas chromatography for rapid workplace hazardous volatile organic compounds measurement, Lab Chip 13 (2013) 818–825.
[26] M. Akbar, S. Narayanan, M. Restaino, M. Agah, A purge and trap integrated microGC platform for chemical identification in aqueous samples, Analyst 139 (2014) 3384–3392.
[27] R.P. Manginell, J.M. Bauer, M.W. Moorman, L.J. Sanchez, J.M. Anderson, J.J. Whiting, D.A. Porter, D. Copic, K.E. Achyuthan, A monolithically-integrated μGC chemical sensor system, Sensors 11 (2011) 6517–6532.
[28] C. Chen, F. Tsow, K.D. Campbell, R. Iglesias, E. Forzani, N. Tao, A wireless hybrid chemical sensor for detection of environmental volatile organic compounds, IEEE Sens. J. 13 (2013) 1748.
[29] R. Haudebourg, J. Vial, D. Thiebaut, K. Danaie, J. Breviere, P. Sassiat, I. Azzouz, B. Bourlon, Temperature-programmed sputtered micromachined gas chromatography columns: an approach to fast separations in oilfield applications, Anal. Chem. 85 (2012) 114–120.
[30] J. Sun, D. Cui, X. Chen, L. Zhang, H. Cai, H. Li, Fabrication and characterization of microelectromechanical systems-based gas chromatography column with embedded micro-posts for separation of environmental carcinogens, J. Chromatogr. A 1291 (2013) 122–128.
[31] V. Lindroos, S. Franssila, M. Tilli, M. Paulasto-Krockel, A. Lehto, T. Motooka, V.-M. Airaksinen, Handbook of Silicon Based MEMS Materials and Technologies, Elsevier, 2009.
[32] M. Stadermann, A.D. McBrady, B. Dick, V.R. Reid, A. Noy, R.E. Synovec, O. Bakajin, Ultrafast gas chromatography on single-wall carbon nanotube stationary phases in microfabricated channels, Anal. Chem. 78 (2006) 5639–5644.
[33] H. Shakeel, M. Agah, Self-patterned gold-electroplated multicapillary gas separation columns with MPG stationary phases, J. Microelectromech. Syst. 22 (2013) 62–70.
[34] S. Reidy, G. Lambertus, J. Reece, R. Sacks, High-performance, static-coated silicon microfabricated columns for gas chromatography, Anal. Chem. 78 (2006) 2623–2630.
[35] B. Alfeeli, S. Narayanan, D. Moodie, P. Zellner, M. McMillan, D. Hirtenstein, G. Rice, M. Agah, Inter-channel mixing minimization in semi-packed micro gas chromatography columns, IEEE Sens. J. 13 (2013) 4312–4319.
[36] M.A. Zareian-Jahromi, M. Agah, Microfabricated gas chromatography columns with monolayer-protected gold stationary phases, J. Microelectromech. Syst. 19 (2010) 294–304.
[37] A.D. Radadia, R.D. Morgan, R.I. Masel, M.A. Shannon, Partially buried microcolumns for micro gas analyzers, Anal. Chem. 81 (2009) 3471–3477.
[38] M. Agah, K.D. Wise, Low-mass PECVD oxynitride gas chromatographic columns, IEEE J. Microelectromech. Syst. 16 (2007) 853–860.
[39] H. Shakeel, D. Wang, J.R. Heflin, M. Agah, Width-modulated microfluidic columns for gas separations, IEEE Sens. J. 14 (2014) 3352–3357.
[40] S. Ali, M. Ashraf-Khorassani, L.T. Taylor, M. Agah, MEMS-based semi-packed gas chromatography columns, Sens. Actuators, B: Chem. 141 (2009) 309–315.
[41] H. Shakeel, G.W. Rice, M. Agah, Semipacked columns with atomic layer-deposited alumina as a stationary phase, Sens. Actuators, B: Chem. 203 (2014) 641–646.
[42] R. Haudebourg, Z. Matouk, E. Zoghlami, I. Azzouz, K. Danaie, P. Sassiat, D. Thiebaut, J. Vial, Sputtered alumina as a novel stationary phase for micro machined gas chromatography columns, Anal. Bioanal. Chem. 406 (2014) 1245–1247.
[43] J. Vial, D. Thiébaut, F. Marty, P. Guibal, R. Haudebourg, K. Nachef, K. Danaie, B. Bourlon, Silica sputtering as a novel collective stationary phase deposition for microelectromechanical system gas chromatography column: Feasibility and first separations, J. Chromatogr. A 1218 (2011) 3262–3266.
[44] J. Sun, D. Cui, F. Guan, X. Chen, L. Zhang, High resolution microfabricated gas chromatography column with porous silicon acting as support, Sens. Actuators, B: Chem. 201 (2014) 19–24.
[45] Y. Li, X. Du, Y. Wang, H. Tai, D. Qiu, Q. Lin, Y. Jiang, Improvement of column efficiency in MEMS-based gas chromatography column, RSC Adv. 4 (2014) 3742–3747.
[46] A.D. Radadia, R.I. Masel, M.A. Shannon, J.P. Jerrell, K.R. Cadwallader, Micromachined GC columns for fast separation of organophosphonate and organosulfur compounds, Anal. Chem. 80 (2008) 4087–4094.
[47] M. Akbar, H. Shakeel, M. Agah, GC-on-chip: integrated column and photoionization detector, Lab Chip (2015), http://dx.doi.org/10.1039/c4lc01461h
[48] D. Wang, H. Shakeel, J. Lovette, G.W. Rice, J.R. Heflin, M. Agah, Highly stable surface functionalization of microgas chromatography columns using layer-by-layer self-assembly of silica nanoparticles, Anal. Chem. 85 (2013) 8135–8141.
[49] M. Akbar, D. Wang, H. Shakeel, J.R. Heflin, M. Agah, A MEMS enabled integrated microGC platform for on-site monitoring of water organic compounds, in: IEEE Transducers Barcelona, Spain, 2013, pp. 2759–2762.
[50] B. Alfeeli, S. Ali, V. Jain, R. Montazami, J. Heflin, M. Agah, MEMS-based gas chromatography columns with nano-structured stationary phases, in: Sensors, 2008 IEEE, 2008, pp. 728–731.
[51] H. Shakeel, M. Agah, Semipacked separation columns with monolayer protected gold stationary phases for microgas chromatography, in: Sensors, 2012 IEEE, 2012, pp. 1–4.
[52] S. Franssila, Introduction to Microfabrication, John Wiley & Sons, 2010.
[53] H. Shakeel, G. Rice, M. Agah, First reconfigurable MEMS separation columns for micro gas chromatography, in: Micro Electro Mechanical Systems (MEMS), 2012 IEEE 25th International Conference on, 2012, pp. 823–826.
[54] A. Ulman, Formation and structure of self-assembled monolayers, Chem. Rev. 96 (1996) 1533–1554.
[55] H.M. McNair, J.M. Miller, Basic Gas Chromatography, John Wiley & Sons, 2011.

Biographies

Hamza Shakeel received his B.S. degree in electronic engineering from Ghulam Ishaq Khan Institute of Engineering Sciences and Technology (GIKI), Topi, Pakistan, in 2004, and the M.S. degree in electrical engineering from the University of Maryland, College Park, USA in 2010. He completed his Ph.D. degree at the Virginia Tech MEMS Laboratory, Bradley Department of Electrical and Computer Engineering, Blacksburg in January, 2015. His research interests include micro and nano fabrication techniques, chemical sensors and application of nanomaterials for gas sensing applications.

Dong Wang received his B.S. and M.S. degrees in Applied Physics from University of Science and Technology of China in 2004 and 2007. He completed his PhD majoring in Experimental Condensed Matter Physics at Virginia Tech in 2014. His research interest includes nanostructured thin film coatings and their application on ion-conductive polymer electromechanical bending actuators/sensors and micro gas chromatography devices.

Prof. James R. Heflin received his Ph.D. in Physics from University of Pennsylvania in 1990 and is a Professor of Physics and Associate Director of the Center for Self-Assembled Nanostructures and Devices at Virginia Tech, where he has been a faculty member since 1992. His research focuses on self-assembly of organic optoelectronic materials and devices, an area in which he holds three patents and has published 130 papers. He is co-editor of the textbook "Introduction to Nanoscale Science and Technology," is an Associate Editor of International Journal of Nanoscience, and is leading the development of the Bachelor of Science in Nanoscience degree at Virginia Tech. Prof. Heflin is also co-founder and Chief Technology Officer of the company Virginia nanoTech.

Masoud Agah received his B.S. and M.S. degrees in electrical engineering from Sharif University of Technology (SUT), Iran, in 1996 and 1998, respectively, and his Ph.D. degree from the University of Michigan, Ann Arbor, in 2005. He began his undergraduate studies in 1992 after being awarded by the President of Iran for achieving the first rank in the Nationwide Iranian University Entrance Examination. During his studies, he received numerous awards, including the Iranian Exemplary Graduate Student Honor, awarded by President Khatami in 1998. In 2000, he joined the NSF Center for Wireless Integrated MicroSystems (WIMS ERC), University of Michigan, where he developed MEMS-based gas chromatography columns for environmental monitoring applications. He joined the faculty of Virginia Tech in August 2005, where he is currently an associate professor in the Bradley Department of Electrical and Computer Engineering with a courtesy appointment in the Department of Mechanical Engineering. He is also a core faculty member of Virginia Tech-Wake Forest School of Biomedical Engineering and Sciences. He established the VT MEMS Laboratory in 2005 and has focused his research on environmental and biomedical applications of MEMS and nanotechnology. He is a senior member of the Institute of Electrical and Electronic Engineers (IEEE) and a member of the American Society for Mechanical Engineers (ASME).